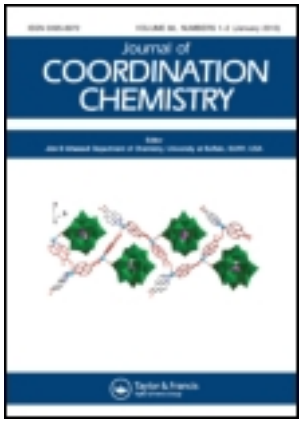

Journal of Coordination Chemistry
Publication details, including instructions for authors and subscription information:
http://www.tandfonline.com/loi/gcoo20

Cobalt 2-pyrazinephosphonates: syntheses, structures, and magnetic properties

Yun-Sheng Ma [a b], Rong-Rong Lv [a], Wang-Shui Cai [a], Meng-Fei Jin [a], Xiao-Yan Tang [a] & Rong-Xin Yuan [a]

[a] School of Chemistry and Materials Engineering, Jiangsu Key Laboratory of Advanced Functional Materials, Changshu Insititute of Technology, Changshu, P.R. China

[b] State Key Laboratory of Coordination Chemistry, School of Chemistry and Chemical Engineering, Nanjing University, Nanjing, P.R. China

Accepted author version posted online: 12 Mar 2013.Published online: 19 Apr 2013.

To cite this article: Yun-Sheng Ma, Rong-Rong Lv, Wang-Shui Cai, Meng-Fei Jin, Xiao-Yan Tang & Rong-Xin Yuan (2013) Cobalt 2-pyrazinephosphonates: syntheses, structures, and magnetic properties, Journal of Coordination Chemistry, 66:9, 1497-1507, DOI: 10.1080/00958972.2013.783908

To link to this article: http://dx.doi.org/10.1080/00958972.2013.783908

Journal of Coordination Chemistry, 2013
Vol. 66, No. 9, 1497–1507, http://dx.doi.org/10.1080/00958972.2013.783908

Cobalt 2-pyrazinephosphonates: syntheses, structures, and magnetic properties

YUN-SHENG MA*†,‡, RONG-RONG LV†, WANG-SHUI CAI†, MENG-FEI JIN†, XIAO-YAN TANG† and RONG-XIN YUAN*†

†School of Chemistry and Materials Engineering, Jiangsu Key Laboratory of Advanced Functional Materials, Changshu Insititute of Technology, Changshu, P.R. China
‡State Key Laboratory of Coordination Chemistry, School of Chemistry and Chemical Engineering, Nanjing University, Nanjing, P.R. China

(*Received 22 June 2012; in final form 10 January 2013*)

Reactions of $Co(ClO_4)_2{\cdot}6H_2O$ with 2-pyrazinephosphonic acid (2-paPO_3H_2) under two different hydrothermal conditions gave two new cobalt 2-pyrazinephosphonates, Co(2-pa$PO_3H)_2$ (**1**) and Co(2-paPO_3)(H_2O) (**2**). Compound **1** was obtained at 160 °C, while **2** was obtained at 180 °C. In **1**, two Co(II) units are bridged by two O–P–O's into a dimer and the dimers are linked by pyrazinyl groups into a 1-D double chain. In **2**, the $\{CoO_4N_2\}$ and $\{CPO_3\}$ polyhedra are interconnected via edge and corner-sharing into a metal phosphonate layer, and the layers are pillared by pyrazinyl groups into a 3-D network. Variable-temperature magnetic susceptibility studies reveal that both complexes have weak antiferromagnetic coupling between Co(II) ions.

Keywords: Cobalt; Phosphonate; Polymer; Magnetic

1. Introduction

Crystal engineering has become an intense research activity because of the growing need for solid-state architectures with potential applications as functional materials in zeolitic behavior, catalysis, and magnetism [1–4]. Selection of terminal ligands is a key step for design of metal–organic coordination polymers with topologies having specific chemical and physical properties [5–7]. Pyrazine is a highly attractive bridging ligand due to its lone pairs on the nitrogen atoms, through which it may coordinate to metal centers [8]. The carboxylate attached pyrazine (2-pyrazinecarboxylate, L) has been used for synthesis of different complexes with N- and O-donors. The potential for coordination and hydrogen bonding interaction of the ligand can lead to various molecular or supramolecular architectures. These include homometallic complexes such as 1-D $[CoNa(N_3)_2L]$ showing single-chain magnet behavior [9]. 2-D $[Ln_2(C_2O_4)_2(L)_2(H_2O)_2]$ displays liquid-state luminescent emission [10]. The more interesting complexes are heterometallic 3-D polymers $[Co_4(L)_4(V_6O_{17})]$ and $[Ni_4(L)_4(V_6O_{17})]$ that are chiral and stable at 400 °C [11].

*Corresponding author. Emails: myschem@cslg.edu.cn (Y.-S. Ma); yuanrx@cslg.edu.cn (R.-X. Yuan)

Monophosphonic acid RPO_3H_2, where R represents an alkyl or aryl group, prefer to form layered lattices or cage-like structures with transition metals [12,13]. To obtain complexes with new structures and properties, functional groups such as amino, aza-crown, sulfonate, and pyridyl have been introduced to the phosphonate [14–17]. The pyrazinephosphonic acid incorporates both pyrazine and phosphonate. Presence of the 2-phosphonate on the pyrazine ring furnishes additional potential for chelation. Together, the oxygen and nitrogen atoms, and their arrangement in space generate a ligand that can simultaneously bridge in many different modes generating three polymers [Zn(2-paPO$_3$)], Cd[(2-paPO3)(H2O)], and Cd[(2-paPO$_3$H)Cl] [18]. In [Zn(2-paPO$_3$)], the O–P–O bridged inorganic layers are pillared by pyrazinyl groups into a 3-D network. In Cd[(2-paPO$_3$)(H$_2$O)], {CdO$_5$N} and {CPO$_3$} polyhedra are interconnected via edge and corner-sharing into a metal phosphonate layer, while in Cd[(2-paPO$_3$H)Cl], the {Cd$_2$Cl$_2$} dimers are linked by O–P–O bridges into a 1-D double chain, and the chains are joined into a layer by pyrazinyl groups.

As part of an extended study concerning 2-paPO$_3^{2-}$ for construction of metal polymers, here we report syntheses, crystal structures, and magnetic properties of two cobalt complexes with different compositions: ligand-rich 1 : 2 compound Co(2-paPO$_3$H)$_2$ (**1**) and ligand-deficient 1 : 1 compound Co(2-paPO$_3$)(H$_2$O) (**2**).

2. Experimental

2.1. *Materials and methods*

All starting materials were reagent grade and used as purchased. The 2-paPO$_3$H$_2$ was prepared according to the literature method [19]. Elemental analyses were performed on a PE 240C elemental analyzer. The FT-IR spectra were recorded on a NICOLET 380 spectrometer with pressed KBr pellets. All magnetic studies were performed on the microcrystalline state. Magnetic susceptibilities were measured on a Quantum Design MPMS SQUID-XL7 magnetometer. Diamagnetic corrections were made for both the sample holder and the compound estimated from Pascal's constants [20].

2.2. *Syntheses*

2.2.1. Co(2-paPO$_3$H)$_2$ (1). A mixture of Co(ClO$_4$)$_2$·6H$_2$O (0.0177 g, 0.05 mmol), 2-paPO$_3$H$_2$ (0.0160 g, 0.1 mmol), and H$_2$O (2 mL) was placed in a Teflon-lined stainless steel vessel, adjusted to pH = 1–2 with dilute HCl, heated at 160 °C for three days, and then cooled to room temperature over 12 h. Pale-yellow block crystals of **1** were obtained with 43% yield based on Co(ClO$_4$)$_2$·6H$_2$O. Elemental analyses calcd (%) for C$_8$H$_8$CoN$_4$O$_6$P$_2$: C, 25.48; H, 2.14; N, 14.86%. Found: C, 25.03; H, 2.44; O, 14.42%.

2.2.2. Co(2-paPO$_3$)(H$_2$O) (2). A mixture of Co(ClO$_4$)$_2$·6H$_2$O (0.0354 g, 0.1 mmol), 2-paPO$_3$H$_2$ (0.0160 g, 0.1 mmol), and H$_2$O (2 mL) was placed in a Teflon-lined stainless steel vessel, heated at 180 °C for three days, and then cooled to room temperature over 12 h. Red block crystals of **2** were obtained with 62% yield based on Co(ClO$_4$)$_2$·6H$_2$O. Elemental analyses calcd (%) for C$_4$H$_5$CoN$_2$O$_4$P: C, 20.44; H, 2.14; N, 11.92%. Found: C, 20.03; H, 2.54; N, 11.52%.

FT-IR spectra of **1** and **2** exhibit absorptions at 1454 and 1393, and 1452 and 1395 cm^{-1}, respectively, assigned to pyrazinyl. Two types of $\nu_{as}(PO_3)$ are inferred from the presence of peaks at 1158 and 1047, and 1160 and 1048 cm^{-1} for **1** and **2**, respectively [21]. Symmetric stretch $\nu_s(PO_3)$ was observed at 960 and 986 cm^{-1} for **1** and **2**, respectively. The sharp feature at 930 cm^{-1} observed for **1** is assigned to ν(POH) mode. No such bands were observed in **2**. These observations are consistent with the X-ray structural analysis (vide infra). The aforementioned stretching vibrations are shifted to lower values compared to those of free ligand, indicating coordination. The metal–ligand (M–O) strectch is located at 533 and 534 cm^{-1}, respectively.

2.3. *X-ray crystallographic analysis*

Single crystals with dimensions $0.22 \times 0.20 \times 0.18$ mm^3 for **1** and $0.18 \times 0.15 \times 0.12$ mm^3 for **2** were selected for indexing and intensity data collection on a Rigaku SCX mini CCD diffractometer using graphite-monochromated Mo-*K*α radiation ($\lambda = 0.71073$ Å) at room temperature. A hemisphere of data was collected in the θ range 3.46–26.00° for **1** and 3.23–27.48° for **2** using a narrow-frame method with scan widths of 0.03° in ω and an exposure time of 10 s $frame^{-1}$. Numbers of observed and unique reflections are 5691 and 2386 ($R_{int} = 0.0383$) for **1**, and 3240 and 1538 ($R_{int} = 0.0.0577$) for **2**, respectively. Cell parameters were refined by using *CrystalClear* [22] on all observed reflections. The collected data were reduced by using *CrystalClear* and an absorption correction (multi-scan) was applied. The reflection data were also corrected for Lorentz and polarization effects. The structures were solved by direct methods and refined on F^2 by full matrix least squares using SHELXTL [23]. All nonhydrogen atoms were located from the Fourier maps and were refined anisotropically. All hydrogen atoms were refined isotropically, with the isotropic vibration parameters related to the non-hydrogen atom to which they are bonded. Crystallographic and refinement details of **1** and **2** are listed in table 1. Selected bond lengths and angles are given in tables 2 and 3 for **1** and **2**, respectively.

Table 1. Crystal data and structure refinements for **1** and **2**.

Formula	$C_8H_8CoN_4O_6P_2$	$C_4H_5CoN_2O_4P$
M	377.05	235.00
Crystal system	Triclinic	Monoclinic
Space group	$P\bar{1}$	*C* c
a (Å)	7.0649(14)	13.190(3)
b (Å)	7.8510(16)	5.2554(11)
c (Å)	11.680(2)	10.275(2)
α (°)	73.73(3)	90
β (°)	86.88(3)	107.22(3)
γ (°)	78.21(3)	90
V	608.8(2)	680.3(3)
Z	2	4
ρ_{calcd} ($g\,cm^{-3}$)	2.057	2.294
μ (mm^{-1})	1.709	2.727
F(000)	378	468
R_{int}	0.038	0.0577
GoF on F^2	1.02	1.02
R_1, wR_2[a] [$I > 2\sigma(I)$]	0.0409, 0.0935	0.0473, 0.0896
R_1, wR_2 (all data)	0.0587, 0.0994	0.0556, 0.0927
$(\Delta\rho)_{max}$, $(\Delta\rho)_{min}$ (e $Å^{-3}$)	0.386, −0.414	0.510, −0.625

[a] $R_1 = \Sigma||F_o| - |F_c|/\Sigma|F_o|$;
$wR_2 = \{\Sigma w(F_o^2 - F_c^2)^2/\Sigma w(F_o^2)^2\}^{1/2}$.

Table 2. Selected bond lengths (Å) and angles (°) for **1**.[a]

Co1–O1	2.076(2)	Co1–N3	2.204(3)
Co1–O4	2.103(2)	Co1–O3A	2.058(2)
Co1–N1	2.146(3)	Co1–N2B	2.161(3)
P1–O2	1.570(2)	P2–O5	1.573(4)
P2–O6	1.486(3)	O3A–Co1–N2B	87.58(11)
O1–Co1–O4	166.83(10)	O4–Co1–N2B	94.03(12)
O1–Co1–N1	82.26(11)	O3A–Co1–O4	93.17(10)
O1–Co1–N3	90.28(11)	N1–Co1–N3	97.10(12)
O1–Co1–N2B	95.06(11)	N1–Co1–N2B	175.21(13)
O1–Co1–O3A	96.70(10)	O3A–Co1–N1	88.79(11)
O4–Co1–N1	89.29(12)	N2B–Co1–N3	86.86(12)
O4–Co1–N3	80.73(11)	O3A–Co1–N3	171.43(11)

[a]Symmetry code: A $1-x, 2-y, 2-z$; B $1+x, y, z$.

Table 3. Selected bond lengths (Å) and angles (°) for **2**.[a]

Co1–O1	2.061(4)	Co1–O2B	2.086(4)
Co1–O4	2.212(4)	Co1–O3A	2.061(4)
Co1–N1	2.154(6)	Co1–N2C	2.181(5)
O1–Co1–O4	170.63(16)	O2B–Co1–O4	82.99(15)
O1–Co1–N1	82.40 (18)	O4–Co1–N2C	93.81(17)
O1–Co1–O3A	96.01(16)	O3A–Co1–N1	86.32(18)
O1–Co1–O2B	93.64(16)	O2B–Co1–N1	86.14(18)
O1–Co1–N2C	95.14(18)	N1–Co1–N2C	177.5(2)
O4–Co1–N1	88.64(18)	O2B–Co1–O3A	166.86(16)
O3A–Co1–O4	86.10(15)	O3A–Co1–N2C	94.19(18)
O2B–Co1–N2C	93.81(17)		

[a]Symmetry code: A $x, -1+y, z$; B $x, 1-y, -1/2+z$; C $1/2+x, -1/2+y, z$.

3. Results and discussion

3.1. *Syntheses*

Temperature, pH, and molar ratio play important roles in formation of **1**. At 160 °C, with pH of 1 to 4 and with the Co(II):2-paPO$_3$H$_2$ molar ratio of 1 : 2, pure **1** can be obtained. Increasing the Co(II) ion molar ratio to 1 : 1, a mixture of **1** and **2** was obtained. Lowering the temperature, **1** and a pale-orange precipitate which was not characterized were formed. When the temperature was increased to 180 °C, pure **2** was obtained no matter what the molar ratio is. This may due to deprotonation and strong coordination ability of the ligand at high temperature.

3.2. *Description of the crystal structure of Co(2-paPO$_3$H)$_2$ (1)*

Single crystal analysis reveals that **1** crystallizes in the triclinic space group $P\bar{1}$. The asymmetric unit consists of one Co(II) and two 2-paPO$_3$H$^-$ (figure 1). The Co(II) adopts distorted octahedral {CoO$_3$N$_3$} coordination, formed by coordination of four 2-paPO$_3$H$^-$. The Co(1)–O distances are 2.058(2)–2.103(2) Å, similar to those found for cobalt phosphonates [24], whereas Co(1)–N distances are 2.146(3)–2.204(3) Å, close to those found for pyrazinyl coordinated complexes [11]. Distortion of the {CoO$_3$N$_3$} octahedron is

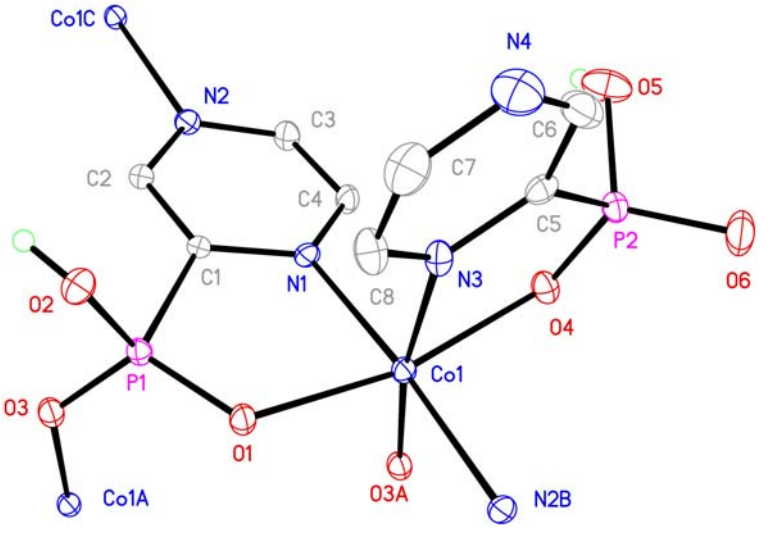

Figure 1. ORTEP drawing of **1** showing 30% probability ellipsoids. Hydrogen atoms attached to carbon are omitted for clarity. Symmetry codes: A $1-x, 2-y, 2-z$; B $1+x, y, z$; C $x-1, y, z$.

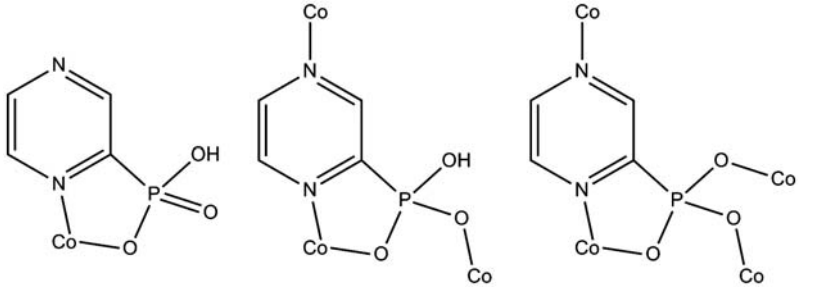

Scheme 1. The coordination modes of the ligand.

mainly due to the small bite of 2-paPO$_3$H$^-$ of about 80°. Two equivalent Co(II) ions are bridged by two O–P–O into a dimer with Co(1)···Co(1A) distance of 4.989(2) Å. The dimers are bridged by pyrazinyl groups into a 1-D double chain (figure S1). The Co(1)···Co (1C) distance over pyrazinyl is 7.065(2) Å. One 2-paPO$_3$H$^-$ is bidentate chelating, while the other is tetradentate bridging (scheme 1). The chains are linked through hydrogen bonding interactions [O(2)···O(6): 2.493(4) Å, 170(5)°, symmetry code: x − 1, y + 1, z; O(5)···O(2): 2.762(4) Å, 158(4)°, symmetry code: x, y − 1, z] into a layer (figure 2).

3.3. *Description of the crystal structure of Co(2-paPO$_3$)(H$_2$O) (2)*

Compound **2** crystallizes in monoclinic space group *C*c. The asymmetric unit consists of one Co(II), one 2-paPO$_3^{2-}$, and one coordinated water (figure 3). The Co(II) is distorted octahedral {CoO$_4$N$_2$}. Five of the six coordination sites are filled with phosphonate oxygen/nitrogen atoms (O(1), O(3A), O(2B), N(1), N(2C)) from four equivalent 2-paPO$_3^{2-}$

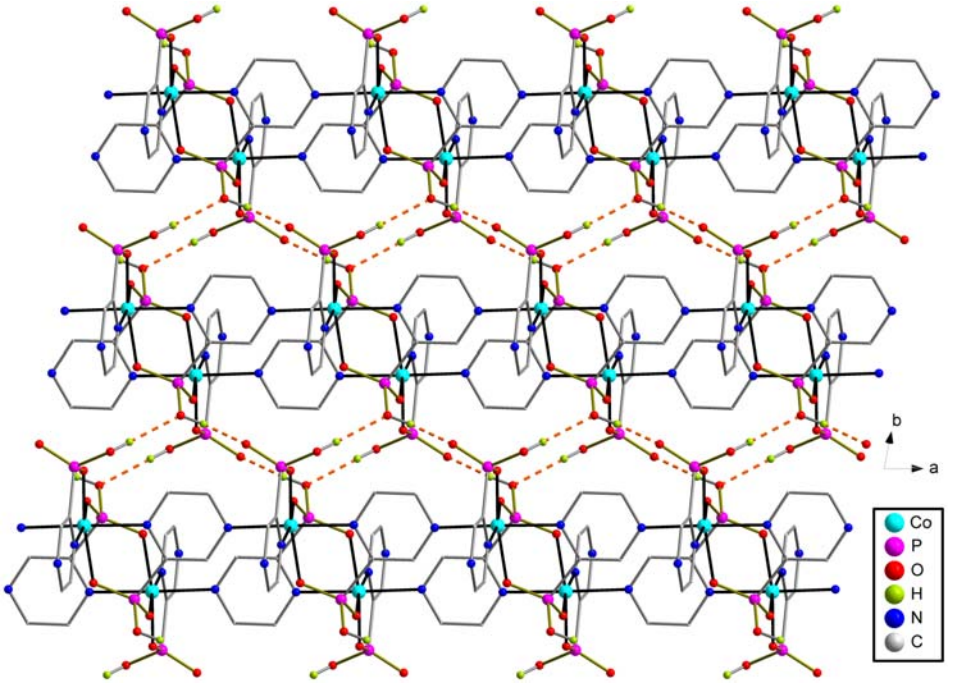

Figure 2. Hydrogen bond connected 2-D network of **1** viewed along the *c*-axis.

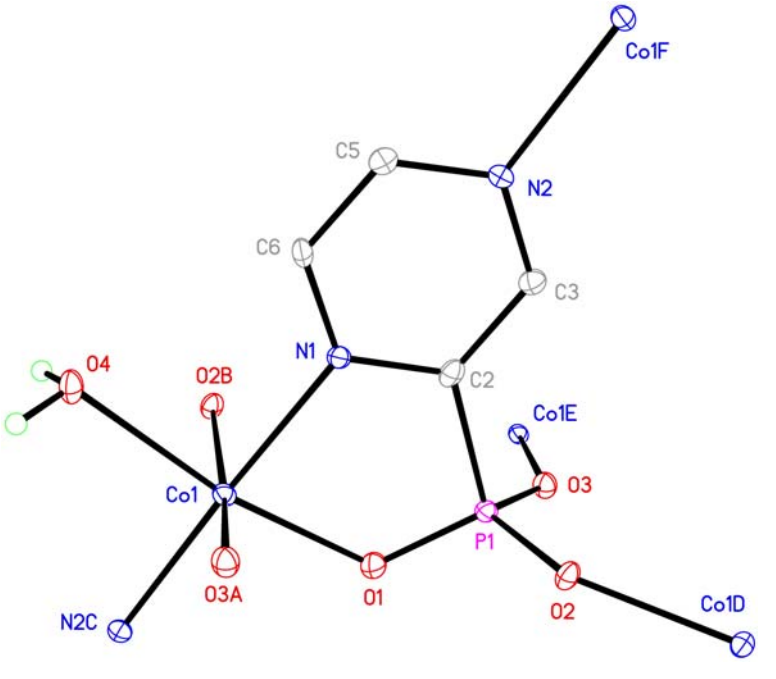

Figure 3. ORTEP drawing of **2** showing 30% probability ellipsoids. Hydrogen atoms attached to carbon are omitted for clarity. Symmetry codes: A $x, y-1, z$; B $x, -y+1, z-1/2$; C $x+1/2, y-1/2, z$; D $x, -y+1, z+1/2$; E $x, y+1, z$; F $x-1/2, y+1/2, z$.

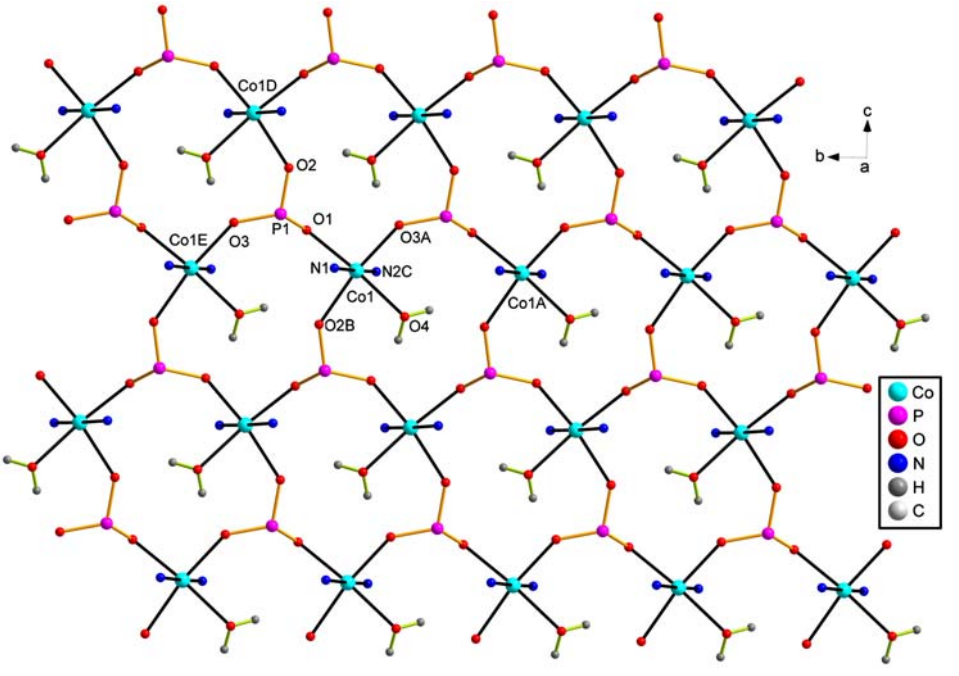

Figure 4. The inorganic layer of **2** viewed along the *a*-axis. All carbon and hydrogen atoms attached to carbon are omitted for clarity.

ligands. The remaining site is occupied by O(4) from water. Co(1)–O bond lengths are 2.061(4)–2.212(4) Å, in agreement with those in **1**. The Co(1)–N distances are 2.154(6) and 2.181(5) Å. The 2-paPO$_3^{2-}$ is pentadentate chelating and bridging, chelating Co(II) ions through phosphonate oxygen O(1) and pyrazinyl nitrogen N(1). Each remaining phosphonate oxygen coordinated to other equivalent Co(II) ions. Consequently, each [CPO$_3$] tetrahedron is vertex-shared with three [CoO$_4$N$_2$] octahedra through three phosphonate oxygen atoms, thus forming an inorganic layer containing 12-membered rings (figure 4). Within the inorganic layer, Co(II) ions are linked purely through O–P–O bridges. The inorganic layer is different from that found in the pillar-layered compound Zn(2-paPO$_3$), where 8- and 16-membered rings may be observed [18]. The Co(1)···Co(1) distances across O–P–O units are 5.255(2), 5.464(1), and 6.158(1) Å, respectively. The layers are pillared by pyrazinyl groups along the *a*-axis into a 3-D network (figure 5).

3.4. *Magnetic properties*

Variable-temperature (1.8–300 K) magnetic susceptibility data at 0.1 *T* were recorded (figures 6 and 7). The $\chi_M T$ product at 300 K of 2.99 and 3.01 cm^3 K mol^{-1} per Co(II) for **1** and **2** are significantly higher than the spin-only value expected for noninteracting ion with $S = 3/2$ (1.875 cm^3 K mol^{-1}). This is attributed to the orbital contribution of Co(II), which is significant in an octahedral field. On lowering the temperature, $\chi_M T$ slowly decreases until 100 K and falls drastically reaching a value of 0.86 and 1.06 cm^3 K mol^{-1} for **1** and **2** at 1.8 K. The continuous decrease in $\chi_M T$ with decreasing temperature is indicative of antiferromagnetic interactions; however, orbital contributions cannot be

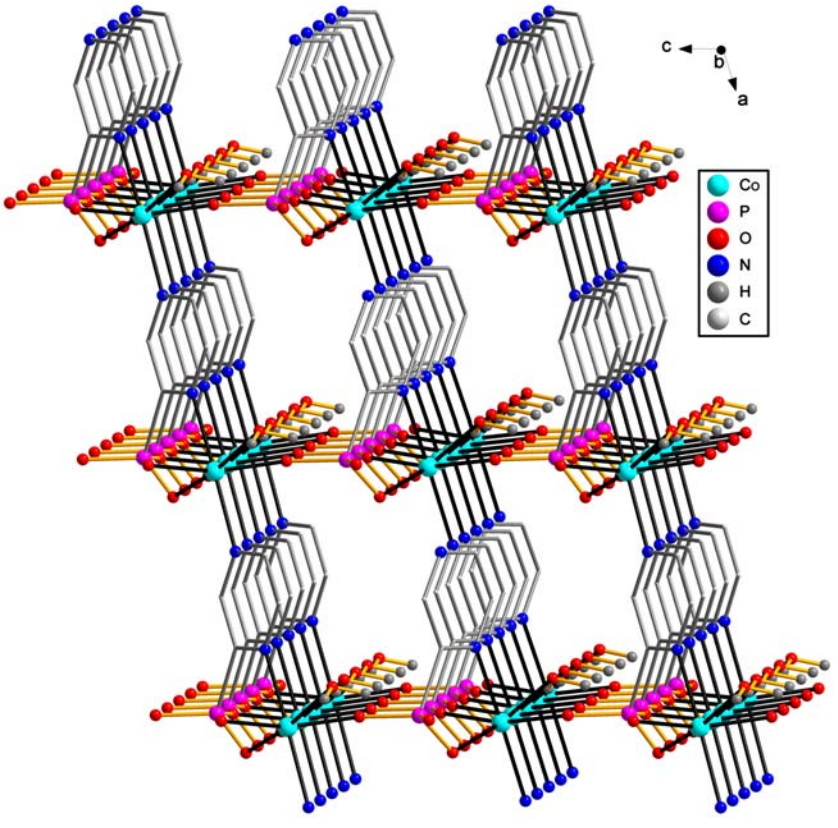

Figure 5. 3-D structure of **2**. All hydrogen atoms attached to carbon are omitted for clarity.

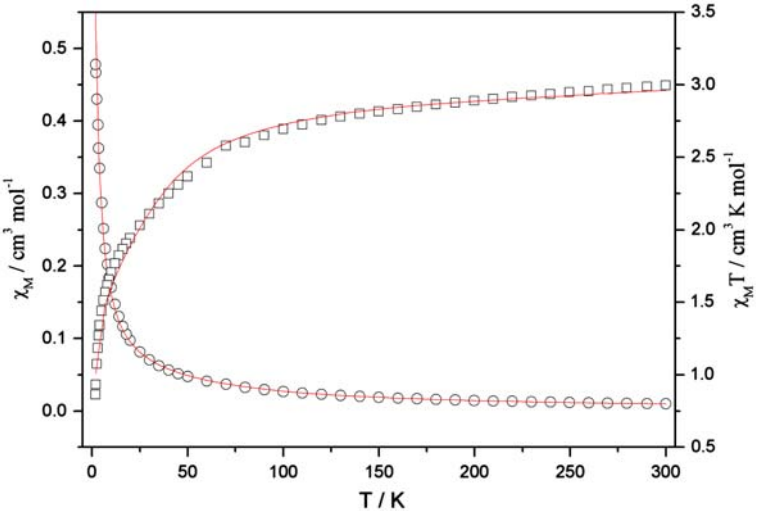

Figure 6. Plots of χ_M *vs.* T and $\chi_M T$ *vs.* T for **1**. The solid lines correspond to the best fit obtained with eq. (1) for **1**.

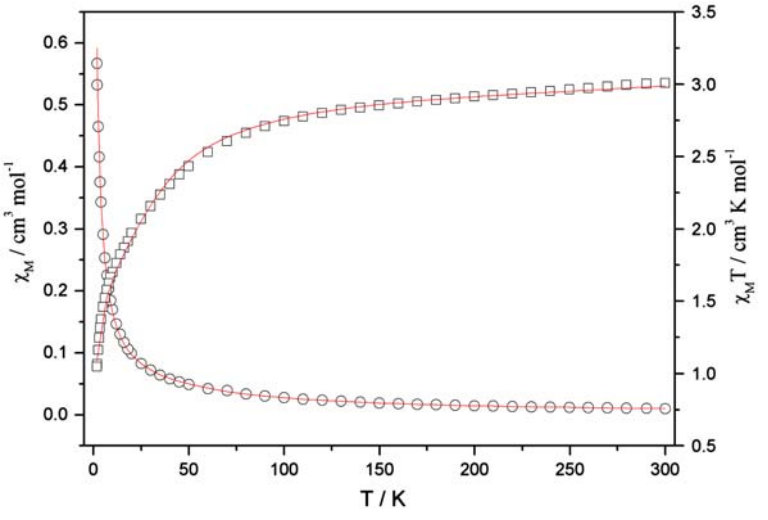

Figure 7. Plots of χ_M *vs.* T and $\chi_M T$ *vs.* T for **2**. The solid lines correspond to the best fit obtained with eq. (1) for **2**.

discarded and also influence the overall profile. The Curie–Weiss fitting of $1/\chi_M$ from 25–300 K gives a good result with Weiss constant, $\theta = -16.47$ K for **1** and $\theta = -14.25$ K for **2**, and the Curie constant, $C = 3.14$ cm^3 K mol^{-1} for **1** (figure S2) and $C = 3.13$ cm^3 K mol^{-1} for **2** (figure S3). The negative θ value indicates antiferromagnetic interactions and/or strong spin-orbital coupling effect of Co(II).

In order to further estimate the strength of the antiferromagnetic exchange interaction as well as the spin-orbital coupling, we treat the magnetic data by considering a mononuclear Co(II) in an octahedral environment. The data were fitted using equation (1) [25],

$$\chi_{Co} = \frac{N\beta^2}{k(T-\theta)x} \frac{\begin{array}{c}\dfrac{7(3-A)^2x}{5} + \dfrac{12(A+2)^2}{25A} + \left\{\dfrac{2(11-2A)^2x}{45} + \dfrac{176(A+2)^2}{675A}\right\}\exp(-5Ax/2) \\ + \left\{\dfrac{(A+5)^2x}{9} - \dfrac{20(A+2)^2}{27A}\right\}x\exp(-4Ax)\end{array}}{3 + 2\exp(-5Ax/2) + \exp(-4Ax)} \quad (1)$$

with $x = \lambda/k_B T$. The parameter A gives a measure of the crystal field strength relative to the interelectronic repulsions and is equal to 1.5 for a weak crystal field, 1.32 for a free ion, and 1.0 for a strong field. In eq. (1), N, β, k_B, T, and θ have their usual meanings. The best fitting of the susceptibility data in the full temperature range gives $\lambda = -77.88$ cm^{-1}, $A = 1.13$, and $\theta = -1.06$ K for **1**, and $\lambda = -74.36$ cm^{-1}, $A = 1.14$, and $\theta = -0.88$ K for **2**. The small negative θ indicates weak antiferromagnetic coupling between the Co(II) ions bridged by O–P–O groups.

From the structural point of view, the superexchange pathway produced by O–P–O of 2-paPO$_3^{2-}$ could be responsible for the magnetic behavior for **1** and **2**. Indeed, it is common to observe that O–P–O bridges transfer antiferromagnetic interactions in metal phosphonates [13]. As observed in the structures, the nearest Co···Co distance of 4.989

(2) Å for **1** is shorter than the distance of 5.255(2) Å for **2**; this may lead to the slightly stronger antiferromagnetic interactions in **1**.

4. Conclusions

The complexes reported herein reveal the versatility of the bridging 2-paPO$_3^{2-}$ to Co(II) (scheme 1), a versatility that provides access to the interesting supramolecular structures that are stabilized through hydrogen bonding interactions. The 1-D double chain structure of **1** is different from that of other metal diphosphonates such as [Co(hedpH$_2$)$_2$](4,4′-bipyH$_2$)·(H$_2$O) and [Cu(H$_5$ahdp)·H$_2$O]$_n$. In the latter compounds, metal ions are connected by O–P–O into one chain. Hydrogen bonds link the chains into a 3-D network [26]. The pillar-layered structure of **2** is different from the 3-D structure of NaCo[O$_3$PCH(OH)CO$_2$]. The latter has a 3-D open framework with channels running along the *a*-axis and Na$^+$ cations located at the intersection of these channels [27]. The magnetic property studies indicate that weak antiferromagnetic interactions are propagated between Co(II) centers in **1** and **2**. Antiferromagnetic interactions between Co(II) ions have been observed in Co(2-mpac)$_2$(H$_2$O)$_2$ and [Co$_3$L$_6$(H$_2$O)$_6$](ClO$_4$)$_6$ [28]. Further work is in progress to obtain new metal 2-pyrazinephosphonates by systematic exploration of synthetic parameters.

Supplementary material

CCDC 860939 and 860940 contain the supplementary crystallographic data for this paper. These data can be obtained free of charge from the Cambridge Crystallographic Data Center via www.ccdc.cam.ac.uk/data_request/cif. Figure S1: 1-D double chain structure of **1**. Figure S2: $1/\chi$ *vs*. *T* curve for **1**. Figure S3: $1/\chi$ *vs*. *T* curve for **2**.

Acknowledgments

This work is supported by NSFC (No. 21001018), NSF of Jiangsu Provence (No. BK2012643, No. 12KJA 150001, 11KJB 150001), the State Key Laboratory of Coordination Chemistry of Nanjing University, and Qinglan Project of Jiangsu Province.

References

[1] C. Janiak. *Dalton Trans*., 2781 (2003).
[2] Z. Wang, G. Chen, K. Ding. *Chem. Rev.*, **109**, 322 (2009).
[3] J. Galezowska, E. Gumienna-Kontecka. *Coord. Chem. Rev.*, **256**, 105 (2012).
[4] K. Maeda. *Micropor. Mesopor. Mater.*, **73**, 47 (2004).
[5] J.-P. Zhang, X.-C. Huang, X.-M. Chen. *Chem. Soc. Rev.*, **38**, 2385 (2009).
[6] S.R. Batten, K.S. Murray. *Coord. Chem. Rev.*, **246**, 103 (2003).
[7] G.K.H. Shimizu, R. Vaidhyanathan, J.M. Taylor. *Chem. Soc. Rev.*, **38**, 1430 (2009).
[8] J.M. Ellswoeth, H.C. zur Loye. *Dalton Trans*., 5823 (2008).
[9] B.-W. Hu, J.-P. Zhao, Q. Yang, X.-F. Zhang, M. Evangelisti, E.C. Sanudo, X.-H. Bu. *Dalton Trans.*, **39**, 11210 (2010).
[10] B. Li, W. Gu, L.-Z. Zhang, J. Qu, Z.-P. Ma, X. Liu, D.-Z. Liao. *Inorg. Chem.*, **45**, 10425 (2006).
[11] L.-M. Zheng, T. Whitfield, X. Wang, A.J. Jacobson. *Angew. Chem. Int. Ed.*, **39**, 4528 (2000).

[12] (a) A. Clearfield. *Prog. Inorg. Chem.*, **47**, 371 (1998); (b) E. Matczak-Jon, V. Videnova-Adrabinska. *Coord. Chem. Rev.*, **249**, 2458 (2005); (c) K.J. Gagnon, H.P. Perry, A. Clearfield. *Chem. Rev.*, **112**, 1034 (2012); (d) J. Galezowska, E. Gumienna-Kontecka. *Coord. Chem. Rev.*, **256**, 105 (2012).
[13] (a) S. Langley, M. Helliwell, R. Sessoli, S.J. Teat, R.E.P. Winpenny. *Dalton Trans*., 3102 (2009); (b) E.I. Tolis, M. Helliwell, S. Langley, J. Raftery, R.E.P. Winpenny. *Angew. Chem. Int. Ed*., **42**, 3804 (2003); (c) M. Wang, C. Ma, C. Chen. *Dalton Trans*., 4612 (2008).
[14] F. Fredoueil, M. Evain, D. Massiot, M. Bojoli-Doeuff, P. Janvier, A. Clearfield, B. Bujoli. *J. Chem. Soc., Dalton Trans*., 1508 (2002).
[15] S.-S. Bao, G.-S. Chen, Y. Wang, Y.-Z. Li, L.-M. Zheng, Q.-H. Luo. *Inorg. Chem.*, **45**, 1124 (2006).
[16] Z.-Y. Du, X.-L. Li, Q.-Y. Liu, J.-G. Mao. *Cryst. Growth Des.*, **7**, 1501 (2007).
[17] Y.-S. Ma, H. Li, J.-J. Wang, S.-S. Bao, R. Cao, Y.-Z. Li, J. Ma, L.-M. Zheng. *Chem. Eur. J.*, **13**, 4759 (2007).
[18] Y.-S. Ma, X.-Y. Tang, W.-Y. Yin, B. Wu, F.-F. Xue, R.-X. Yuan, S. Roy. *Dalton Trans.*, **41**, 2340 (2012).
[19] Y. Belabassi, S. Alzghari, J.-L. Montchamp. *J. Organomet. Chem.*, **693**, 3171 (2008).
[20] O. Kahn. *Molecular Magnetism*, VCH, New York, NY (1993).
[21] L.C. Thomas, R.A. Chittenden. *Spectrochim. Acta*, **20**, 467 (1964).
[22] CrystalClear. Rigaku Corporation, Tokyo, Japan (2005).
[23] G.M. Sheldrick. *Acta Crystallogr., Sect. A: Found. Crystallogr*., **64**, 112 (2008).
[24] Y.-S. Ma, Y. Song, L.-M. Zheng. *Inorg. Chim. Acta*, **361**, 1363 (2008).
[25] H. Zhao, J. Bacsa, A. Prosvirin, N. Lopez, K.R. Dunbar. *Polyhedron*, **24**, 1907 (2005).
[26] (a) J.-F. Xiang, M. Li, S.-M. Wu, L.-J. Yuan, J.-T. Sun. *J. Coord. Chem*., **60**, 1867 (2007); (b) G. Li, Y.-T. Fan, T.-J. Zhang, T.-Z. Ge, H.-W. Hou. *J. Coord. Chem*., **61**, 540 (2008).
[27] L.-Y. Cui, Z.-G. Sun, H. Chen, L. Meng, D.-P. Dong, C.-H. Tian, Z.-M. Zhu, W.-S. You. *J. Coord. Chem.*, **60**, 1247 (2007).
[28] (a) G. Fan, Y.-L. Zhang, J.-J. Sun, M.-Y. Zheng, S.-P. Chen, S.-L. Gao. *J. Coord. Chem*., **63**, 1729 (2010); (b) J. Yang, Y.-S. Ma, X.-Y. Tang, L. Shen, R.-X. Yuan, D.-R. Zhu. *J. Coord. Chem*., **64**, 3291 (2011).